X-ray Photoelectron Spectroscopy Study of Mg Adsorption on Nanocrystalline Hydroxyapatite

Yu. A. Teterin[a, b, *], V. N. Rudin[a], A. V. Severin[a], M. E. Paul'[a], K. I. Maslakov[a],
A. Yu. Teterin[b], and S. V. Dvoryak[a]

[a]Moscow State University, Moscow, 119991 Russia
[b]Kurchatov Institute National Research Centre, pl. Akademika Kurchatova 1, Moscow, 123182 Russia
***e-mail: teterin_ya@yandex.ru**

Abstract—We have studied Mg^{2+} adsorption on hydroxyapatite (HAp) nanocrystals and constructed its isotherm at equilibrium cation concentrations in the range 0–0.35 mol/L. For a number of samples, corresponding to characteristic points in the adsorption isotherm, the composition and the oxidation state of the elements present on the surface of the sorbent have been determined by X-ray photoelectron spectroscopy (XPS). The surface magnesium concentration determined by XPS, which detects only ions in a surface layer a few nanometers in thickness, has been found to be considerably lower than the total amount of cations in the solid phase, evaluated from the experimentally determined adsorption isotherm. We assume that, during the sorption process, some of the magnesium ions substitute for calcium ions in the bulk of the HAp and some adsorb in the form of $MgCl_2$. The results obtained in this study constitute a fundamental basis for practical solutions in designing integrated medications based on HAp with magnesium.

INTRODUCTION

Biological hydroxyapatite (HAp) is a major mineral component of human and animal bone tissue, present in the form of nanocrystals bound to collagen [1]. In connection with this, assessing characteristics of HAp nanocrystals and the state of biologically active molecules and ions adsorbed on their surface remains a topical issue.

A living organism produces biological HAp to be used as a structural component of bone. Synthetic HAp has the same chemical composition as biological HAp ($Ca_{10}(PO_4)_6(OH)_2$) and replicates many properties of natural bone tissue [2, 3]. Besides, bone contains other ions as well, for example, Na^+, Mg^{2+}, K^+, and Cl^-. A special role is played by magnesium ions. The ability to monitor and maintain magnesium homeostasis is important for bone tissue to remain intact. Normally, the structure of bone is constantly remodeled via coordination of interactions between osteoclasts and osteoblasts. Disbalance of their functioning leads to prevalence of bone resorption (disintegration) processes, degradation of the bone structure, decrease in the density of the bone, and, as a consequence, osteoporosis development. Synthetic nanocrystalline HAp per se is successfully used to treat various bone fractures [4]. At the same time, the use of HAp doped with Mg^{2+} ions [2, 3, 5] helps increase the activity of osteoblasts under the effect of the enzyme system of the body, augmenting its reparative capabilities. However, if magnesium is added via cocrystallization [2], its accessibility is markedly lower than in the case of Mg adsorption on the surface of HAp nanocrystals. In connection with this, gaining detailed insight into sorption interaction of magnesium with HAp and its state on the surface of sorbent nanocrystals is a topical issue. The elemental composition and electronic structure of the surface layer of crystals can be assessed by X-ray photoelectron spectroscopy (XPS) [6–8].

The objectives of this work were to study the mechanism of Mg^{2+} adsorption on the surface of HAp nanocrystals [6], construct adsorption isotherms at equilibrium magnesium concentrations from 0 to 0.35 mol/L while determining both the amount of magnesium ions in the surface layer of the sorbent and the oxidation state of the elements present, and estimate the fraction of surface magnesium ions relative to the total amount of magnesium present in the solid phase as a result of the interaction with the HAp.
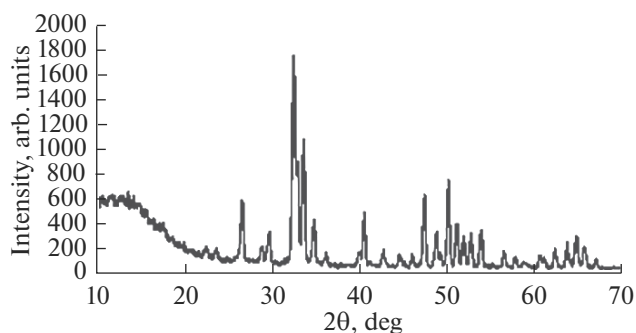
Fig. 1. X-ray diffraction pattern of the nanocrystalline HAp.

EXPERIMENTAL

Nanocrystalline sorbent. The nanosorbent used in this study was an aqueous 5.5% HAp suspension prepared as described by Melikhov et al. [6]. The nanocrystals were on average 62 ± 30 nm in length (l) and 15 ± 7 nm in width (d) and ranged in thickness (h) from one to three crystallographic translations of the unit cell of HAp (~0.8−2.4 nm). The calculated (geometric) specific surface area of the nanocrystals in the suspension was 900 m^2/g, but the actual value was substantially lower, ~170 m^2/g, because of the nanoparticle aggregation [6, 7]. Figure 1 shows the X-ray diffraction pattern of the HAp nanocrystals.

Isotherm of Mg^{2+} adsorption on HAp. In our experiments, a weighed amount of the HAP suspension was placed in a 12-mL vial, and appropriate volumes of magnesium chloride solutions and water were added.

The samples were placed on a SkyLine S-3.08L orbital shaker (Elmi, Latvia) and stirred under identical conditions. After equilibration (for two days), the phases were separated by centrifugation, and the residual magnesium concentration in solution was determined on a Shimadzu UV-1280 spectrophotometer using a wavelength of 540 nm. Magnesium was determined with the use of a specialized reagent containing tris(hydroxymethyl)aminomethane as a major component.

To construct the adsorption isotherm, we obtained 20 data points at a varied HAp : magnesium chloride ratio. The adsorption isotherm thus obtained is shown in Fig. 2 (A is the amount of adsorption in mol Mg/mol HAp, and C_{eq} is the equilibrium Mg concentration, mol/L).

Preparation of samples for XPS characterization. Samples for XPS were prepared as follows: After adsorption equilibrium in the system under study was reached, the mother liquor was separated from the solid phase by centrifugation at 6000g. Next, we took cover glass, degreased its surface with acetone, and applied a small amount of the solid phase left after centrifugation. The HAp nanocrystals were distributed evenly over the cover glass and dried at 50°C. The residual water was removed by rough pumping in a desiccator. As a result, a layer of nanocrystals 1.5 mm in thickness and 7×7 mm^2 in area was produced on the cover glass substrate (10×10 mm). In this manner, the following samples for XPS were prepared: (1) pure HAp (prepared by centrifugation of the starting suspension, (2) HAp-4, (3) HAp-12, (4) HAp-15, and (5)
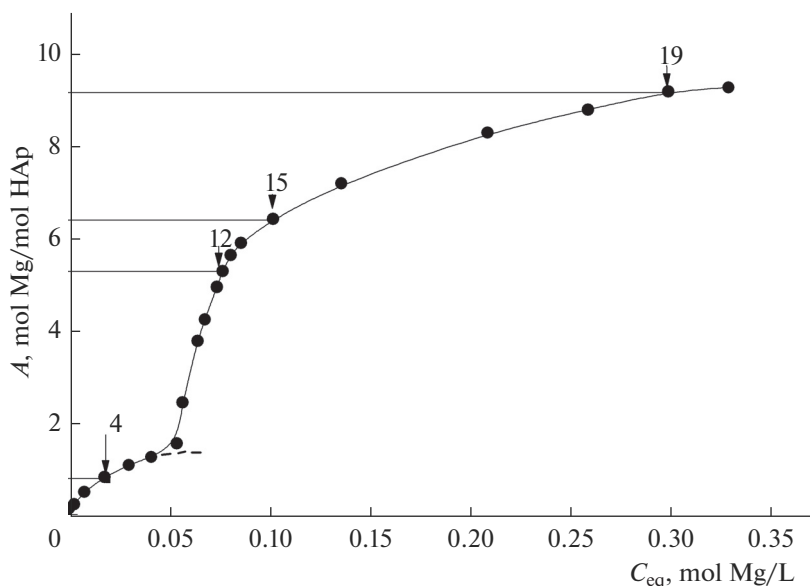

Fig. 2. Isotherm of Mg^{2+} sorption on nanocrystalline HAp from solution: A is the amount of adsorption in mol Mg/mol HAp, and C_{eq} is the equilibrium Mg concentration, mol/L). The arrows mark the data points corresponding to the samples characterized by XPS.

HAp-19 (correspond to data points on the adsorption isotherm in Fig. 2).

XPS measurements. XPS spectra of our samples were obtained on a Kratos Axis Ultra DLD spectrometer using monochromatized Al K_α ($h\nu = 1486.6$ eV) radiation (X-ray tube power of 150 W, vacuum of 1.3×10^{-7} Pa, room temperature). The analysis area was 300×700 μm². The spectrometer was calibrated relative to the position of the Au $4f_{7/2}$ (83.96 eV) and Cu $2p_{3/2}$ (932.62 eV) core levels of pure gold and copper metals. The spectra were collected at a constant analyzer pass energy of 20 eV in 0.05-eV steps. The spectrometer resolution, measured as the full width at half maximum (FWHM) of the Au $4f_{7/2}$ level, was 0.65 eV. As the binding energy (E_b) scale reference, we used the C 1s level (285.0 eV) arising from hydrocarbon contamination adsorbed on the sample surface. The uncertainty in our binding energy and linewidth measurements was within ±0.05 eV, and relative intensities were measured to an accuracy of ±5%. The spectral background due to rescattered electrons was subtracted using the Shirley method [8].

We carried out quantitative elemental analysis of the surface layer of the samples a few nanometers (~3−5 nm [9]) in thickness. It is based on the fact that spectral intensity is proportional to the number of analyte atoms in the sample under study. We used the following relation $n_i/n_j = (S_i/S_j)(k_j/k_i)$, where n_i/n_j is the relative concentration of the atoms of interest, S_i/S_j is the relative spectral intensity, and k_j/k_i is the experimentally determined relative sensitivity factor. In this study, we used the following sensitivity factors relative to C 1s: 1.00 (C 1s), 2.81 (O 1s), 6.59 (Ca 2p), 1.75 (P 2p), 3.21 (Cl 2p), and 8.13 (Mg 1s).

To assign the observed lines in the spectra of HAp and Mg, we used electron binding energies in reference samples: 1304.8 and 51.5 eV for the Mg1s and Mg2p levels in MgCl₂ · 6H₂O, 1302.7 and 49.5 eV for the Mg1s and Mg2p levels in Mg(OH)₂, 1303.9 and 50.8 eV for the Mg1s and Mg2p levels in MgO [11], 346 and 347.3 eV for the Ca2$p_{3/2}$ level in CaO and CaCO₃ [10, 11], and data obtained for MgCl₂ · 6H₂O and Mg(OH)₂ in this study (Table 1). In all cases, we obtained survey and detailed valence band spectra in the range 0−50 eV; the strongest core electron lines of magnesium, calcium, and phosphorus; and the O 1s and C 1s lines of oxygen and carbon.

EXPERIMENTAL RESULTS

The survey XPS scan of nanocrystalline HAp (Ca₁₀(PO₄)₆(OH)₂) (Fig. 3) shows relatively narrow lines of Ca, P, and O atoms at binding energies Eb in the range 0−1250 eV. There are also the C *KLL* and O *KLL* Auger electron lines of carbon and oxygen and the C 1s and Na 1s lines of carbon and sodium. Magnesium adsorption on the surface of nanocrystalline HAp causes the Mg1s, Mg2s, and Mg2p lines to emerge in the survey spectrum; reduces the intensity of the Na 1s line; and produces the main Mg *KLL* Auger electron line at 299.3 eV. Using the intensities of the observed lines and taking into account the relevant relative sensitivity factors, we carried out elemental chemical analysis of the surface of our samples (Table 2).

The valence band and core level electron binding energies and the full widths at half maximum of the corresponding lines are presented in Table 1, together with characteristics of the spectra of the reference samples [10]. The NIST X-ray Photoelectron Spectroscopy Database [11] gives Ca2$p_{3/2}$ electron binding energies of 346.1 eV for CaO and 347.4 eV for CaCO₃, which agree well with data reported by Sosulnikov and Teterin [10].

Figures 3−6 show valence band and core level spectra of some of the samples studied: HAp, HAp-4, HAp-12, HAp-15, and HAp-19.

DISCUSSION

Both the survey XPS scan of HAp and the spectrum of HAp-12 (Fig. 3) show lines of all the constituent elements of hydroxyapatite (Ca₁₀(PO₄)₆(OH)₂) and the C 1s line due to hydrocarbons adsorbed on the sample surface from air. In addition, the spectrum of the HAp-12 sample shows the Mg1s, 2s, and 2p lines due to the adsorbed magnesium (Fig. 3).

The low-energy region in the spectrum of HAp contains lines corresponding to electrons of outer valence molecular orbitals (OVMOs) between 0 and ~15 eV and inner valence molecular orbitals (IVMOs) between ~15 and ~35 eV. The strongest lines are located in the region of the O2s and Ca3p electron binding energies. The structure of the spectrum of OVMO and IVMO electrons in HAp changes slightly upon adsorption of a small amount of magnesium (Fig. 4), as would be expected. The OVMO electron spectrum contains a number of characteristic lines. The Mg3s spectrum of HAp-12 has low intensity compared to the OVMO electron spectrum of HAp (Fig. 4).

In the high-energy region, the OVMO electron spectrum of HAp-12 shows a weak Cl3s line of chlorine (Fig. 4). At binding energies lower than that of the Ca3p level, at 23.1 eV, there is a line due to O2s electrons, involved in chemical bonding and the formation of IVMOs, whereas the O2p states form an outer valence band. The structure of the OVMO electron spectrum is considerably contributed by the P 3s electron states at 12.2 and 23.1 eV, and the P3p electron states contribute to the peak at 9.8 eV. Since the O 2s electrons are involved in chemical bonding, their spectrum is broadened in comparison with the O 1s

Table 1. Electron binding energies (E_b) and full widths at half maximum of XPS lines (Γ) of the samples

Sample	E_b, eV (Γ, eV)						
	Mg2p	Mg1s	Ca 2$p_{3/2,}$	P2p	Cl2$p_{3/2}$	O1s	C1s
HAp	− − −		347.6 (1.2)	133.6 (1.5)		531.4 533.0 (1.2)	285.0 289.0 (1.3)
HAp-4	51.1 (1.2)	1304.4 (1.4)	347.5 (1.1)	133.6 (1.4)	199.0 (1.0)	531.3 533.2 (1.1)	285.0 289.1 (1.3)
HAp-12	51.2 (1.3)	1304.5 (1.4)	347.5 (1.1)	133.6 (1.4)	199.0 (1.0)	531.4 533.2 (1.2)	285.0 289.1 (1.3)
HAp-15	51.2 (1.4)	1304.6 (1.4)	347.6 (1.0)	133.7 (1.4)	199.0 (1.0)	531.6 533.2 (1.1)	285.0 289.2 (1.3)
HAp-19	51.1 (1.4)	1304.6 (1.4)	347.5 (1.1)	133.6 (1.4)	198.9 (1.0)	531.5 533.2 (1.1)	285.0 289.2 (1.3)
MgCl$_2 \cdot$ 6H$_2$O	51.4 (1.4) 51.5*	1304.6 (1.4) 1304.8*			199.1 (1.1)		285.0 (1.3)
Mg(OH)$_2$	49.5*	1302.7*					
MgO	50.8*	1303.9*					
CaO [10]			346.0 (1.7) 346.1*			528.9 (1.4)	285.0
CaCO$_3$ [10]			347.3 (1.7) 347.4*			531.6 (1.6)	285.0 289.7 (1.3)

The binding energies are given relative to E_b(C1s) = 285.0 eV.
* Data borrowed from Ref. [11] (for comparison).

line and comprises a few components. The structure in the region of Ca3p and O2s electrons is related to the participation of their shells in IVMO formation. Magnesium adsorption has little effect on the width of the valence band at the band top (8.6 eV in HAp) and its structure. A similar structure is present in the spectra of the other Mg-containing HAp samples. Probing the valence region, which is a spectral characteristic of the formation of nanocrystalline HAp structure, is important as well for ascertaining that the sample surface is free of unintentional impurities, which might appear during the magnesium adsorption process.

The surface composition of our samples was evaluated using core level binding energies and the intensity of the corresponding lines: Ca2p, P2p, Mg2p, Mg1s, Cl2p, O1s, and C1s (Tables 1, 2). It is worth noting that the Mg2s and Mg2p electron binding energies and the FWHM of the lines of magnesium adsorbed on HAp exceed those of MgO (Table 1). The reason for this is that magnesium in HAp can be bonded to the oxygens of the PO_4^{3-} phosphate groups or surface CO_3^{2-} carbonate groups. The phosphate groups in HAp form stable tetrahedra, in which the state of phosphorus varies little from sample to sample. Indeed, the P2p
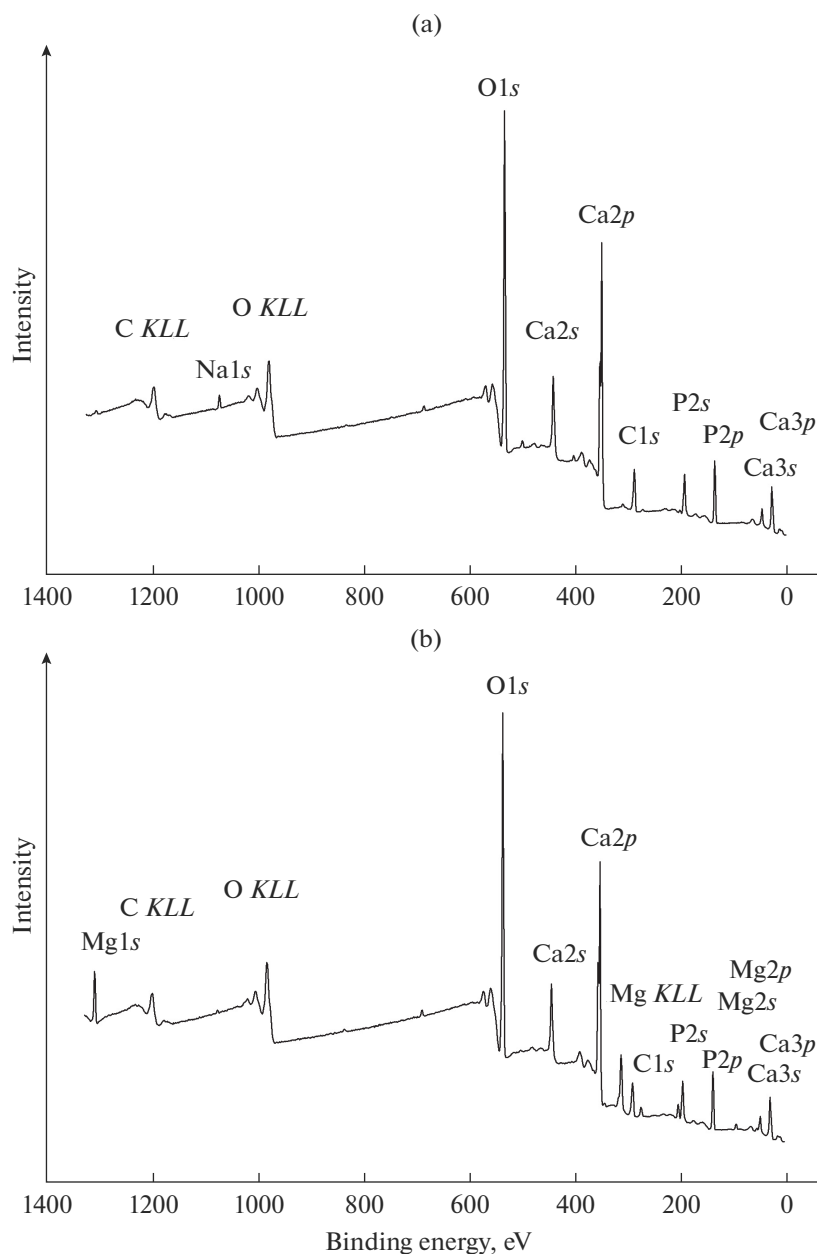
Fig. 3. Survey XPS scans of (a) undoped HAp and (b) the HAp-12 sample (covered with adsorbed Mg).

electron binding energy in HAp is not influenced by magnesium adsorption. Because of this, in quantitative elemental analysis of samples 1−5 we used the intensities of lines of other elements relative to the intensity of the P 2p line (Table 2). In this case, the calcium content of HAp (sample 1) is lower than the calculated one. Note that the experimentally determined composition of HAp coincides with the calculated one to within measurement accuracy (Table 2). Magnesium adsorption further reduces calcium content (samples 2−5). It is reasonable to assume that magnesium partially substitutes for calcium in HAp.

The reference samples (6−10) used to compare their binding energies to those of the samples studied (1−5) were the $MgCl_2$, $Mg(OH)_2$, MgO, CaO, and $CaCO_3$ compounds (Table 1). It is seen from the data in Table 1 that the Mg2p and Mg 1s electron binding energies are most similar to those in $MgCl_2$ and markedly exceed those in $Mg(OH)_2$ and MgO. With increasing magnesium concentration on the surface of the samples (Table 2), the width of the Mg2p line increases markedly (Table 1). In addition, the number of chlorine atoms becomes comparable to that of magnesium atoms (Table 2). This leads us to assume that

Table 2. Atomic surface composition of the samples relative to a P atom at different equilibrium magnesium concentrations

Sample	C_{eq}, mol/L	A, mol Mg/ mol HAp	Surface composition
HAp	—	—	$Ca_{10}P_6O_{24+2}H_2$ (calculation)
	—	—	$Ca_{9.5}P_6O_{25.1+3.4} C_{1.2}$ (experiment)
HAp-4	0.019	0.84	$Ca_{9.2}P_6O_{25.5+5} C_{0.6} Mg_{1.5} Cl_{0.3}$
HAp-12	0.078	5.31	$Ca_{8.8}P_6O_{25.3+2.2} C_{0.1} Mg_{3.1} Cl_{0.9}$
HAp-15	0.103	6.43	$Ca_{9.2}P_6O_{26.0+9.0} C_{1.4} Mg_{3.3} Cl_{3.0}$
HAp-19	0.31	9.19	$Ca_{8.7}P_6O_{26.0+11.8}Cl_{1.5} Mg_{3.0}Cl_{2.6}$

The atomic composition was determined by XPS and is reduced to six phosphorus atoms. The number in the notation of the HAp samples corresponds to its number on the isotherm in Fig. 2.

* For oxygen, we additionally indicate the concentration of atoms belonging to H_2O. Carbon concentration is given for CO_3^{2-} carbonate groups.

the adsorbed magnesium first partially substitutes for calcium atoms in the HAp and that one-tenth of the magnesium is present in the form of $MgCl_2$ (0.15Mg-Cl_2/1.5Mg). Increasing the amount of adsorbed magnesium on the surface of the samples causes about half of the Mg atoms to be present in the form of $MgCl_2$ (Table 1).

The Ca 2p spectrum of HAp has the form of a doublet due to spin−orbit splitting with ΔE_{sl} = 3.5 eV. On the high binding energy side of the Ca2$p_{3/2}$ line, there is a weak satellite (~1%) at 7.8 eV. Magnesium adsorption has no significant effect on the structure of this spectrum (Table 1). The Ca2$p_{3/2}$ electron binding energy in HAp, $E_b(Ca2p_{3/2})$ = 347.6 eV, is essentially constant in all of the samples studied. It exceeds that in CaO and is even slightly higher than that in $CaCO_3$. The Cl2$p_{3/2}$ electron binding energy in the samples studied (2−5) is essentially identical to that in $MgCl_2$ (Table 1).

The C 1s spectra of our samples (1−5) contain, in addition to the weak line at 285.0 eV, due to saturated hydrocarbons on the surface of the samples, a line at ~290.0 eV, due to CO_3^{2-} carbonate groups (Table 1). The carbonate carbon concentration is indicated in Table 2. The carbonate concentration varies from sample to sample, and the carbonate groups can participate in the formation of bonds with magnesium.

The O 1s spectra of our samples contain one main line, with a weak shoulder on its high binding energy side (Fig. 5). This is due to the presence of oxygens of hydroxyl groups and water on the surface of the samples. The binding energy ~531.4 eV corresponds to hydroxyl groups and bridging oxygen ions, predominantly in P−O−P bonds, with a certain contribution from P−O−Ca and P−O−Mg bonds, and the binding energy ~533.0 eV corresponds to water in HAp and on its surface. The concentration of oxygens of the PO_4^{2-} tetrahedra and water, indicated as a sum in Table 2, depends on the amount of magnesium adsorption on HAp. Using the relation
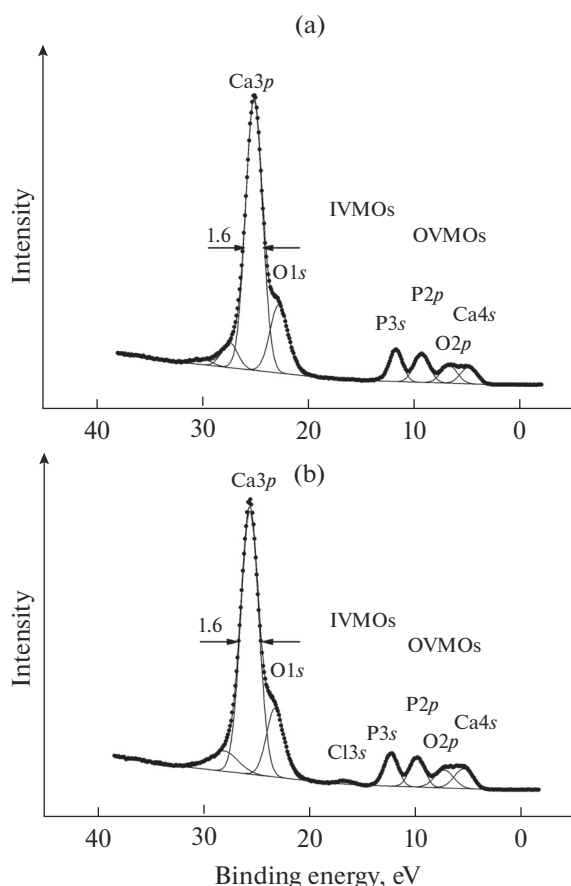
$$R_{E-O} (nm) = 2.27 (E_b - 519.4)^{-1} \qquad (1)$$

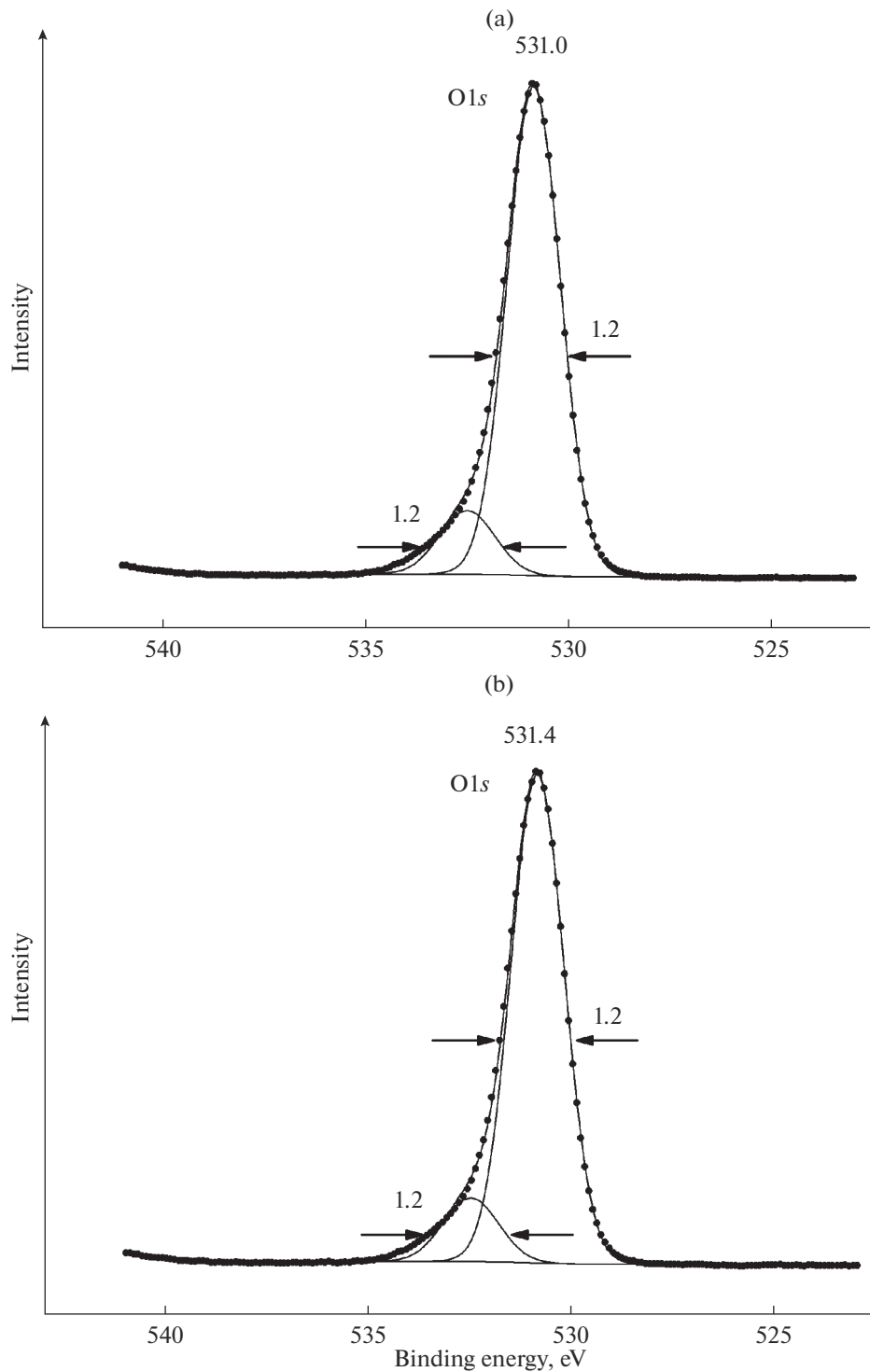**Fig. 4.** Valence band XPS spectra of (a) undoped HAp and (b) the HAp-12 sample (covered with adsorbed Mg).

(a)

531.0

O1s

1.2

1.2

Intensity

540   535   530   525

(b)

531.4

O1s

1.2

1.2

Intensity

540   535   530   525

Binding energy, eV

Fig. 5. O 1s spectra of (a) undoped HAp and (b) the HAp-12 sample (covered with adsorbed Mg).

we estimated element−oxygen R_{E-O} bond lengths. At O 1s electron binding energies of 531.4 and 533.0 eV (Table 1), we obtained 0.189 and 0.167 nm, respectively. These values characterize the element−oxygen bond lengths on the surface of the samples studied.

They were obtained by averaging over all bond lengths (P−O, Ca−O, and Mg−O) in the samples under consideration. Relation (1) was obtained for metal oxides with octahedral coordination, which include MgO, with E_b(O 1s) = 530.1 eV (Table 1). Taking into
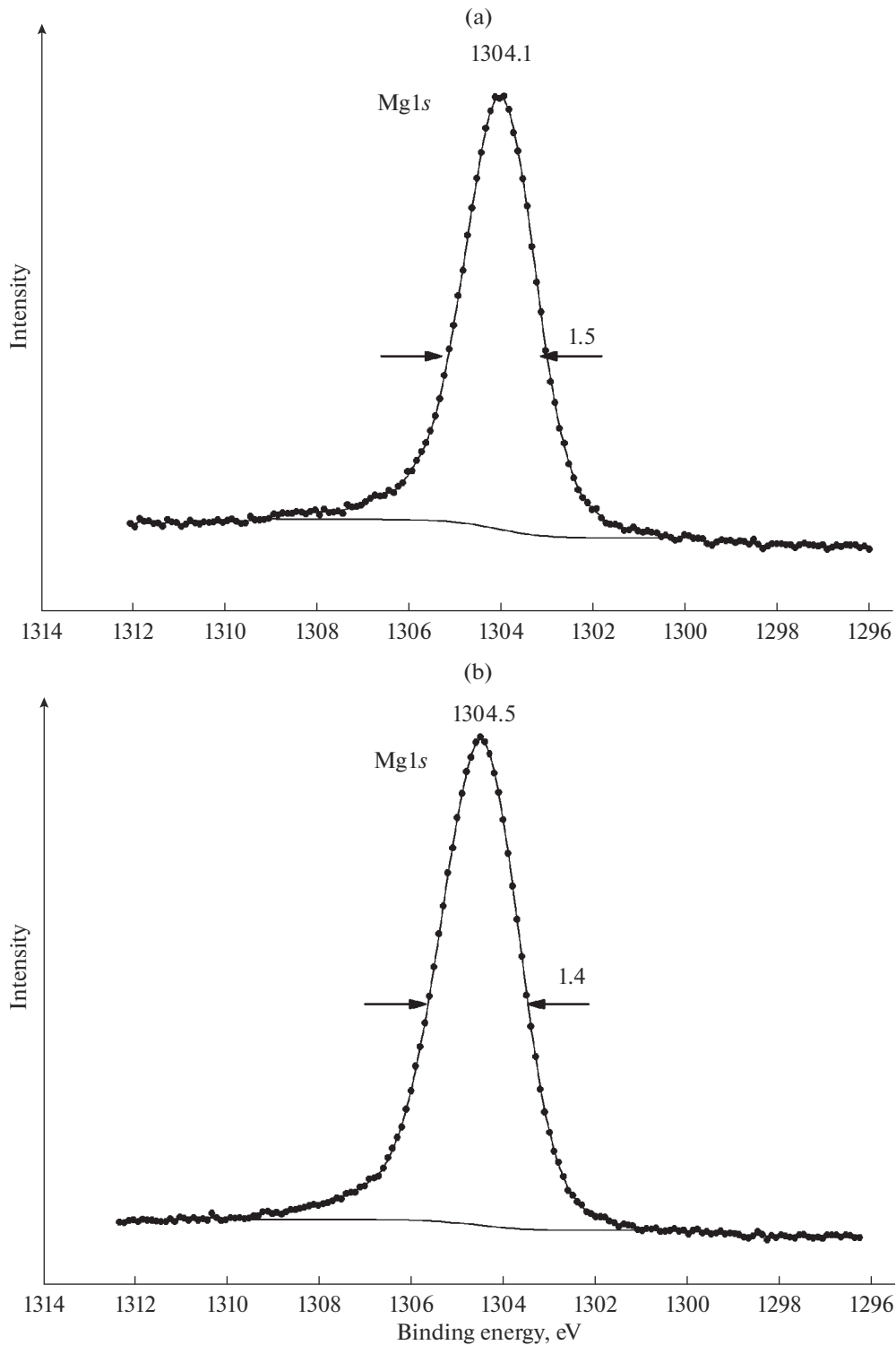
Fig. 6. Mg 1*s* spectra of (a) undoped HAp and (b) the HAp-12 sample (covered with adsorbed Mg).

account relation (1), we find for MgO $R_{Mg-O} = 0.212$ nm. This value is comparable to the sum of the ionic radii $R(O^{2-}) = 0.136$ nm and $R(Mg^{2+}) = 0.074$ nm, equal to 0.210 nm.

CONCLUSIONS

We have studied Mg^{2+} adsorption on HAp nanocrystals and constructed its isotherm at equilibrium magnesium concentrations in the range 0–

0.35 mol/L. For samples corresponding to particular portions of the isotherm, the oxidation state of the elements present on the surface of HAp crystals covered with adsorbed magnesium has been determined by XPS. The data thus obtained have been compared to the adsorption isotherm data.

The results lead us to assume that, in the initial stage of adsorption, the magnesium ions partially substitute for calcium ions in the HAp and that a smaller part of the magnesium adsorbs in the form of $MgCl_2$. With increasing magnesium concentration in solution, the surface magnesium concentration increases and the ratio of the adsorbed magnesium ions to the ions in $MgCl_2$ rises to 1 : 1.

The surface concentration of magnesium ions is substantially lower than that following from the adsorption isotherm, as would be expected. The reason for this is that XPS detects only electrons coming from a depth of a few nanometers, whereas the rest of the magnesium ions in the bulk of the sample remains "invisible" for this method.

The present results provide insight into the mechanism of sorption interaction between nanocrystalline HAp and magnesium ions in a wide range of equilibrium Mg concentrations, which is necessary for producing HAp- and magnesium-based medications.

ACKNOWLEDGMENTS

REFERENCES

1. Melikhov, I.V., Teterin, Yu.A., Rudin, V.N., Teterin, A.Yu., Maslakov, K.I., and Severin, A.V., X-ray study of nano-dispersed hydroxyapatite, *Russ. J. Phys. Chem. A,* 2009, vol. 83, no. 1, pp. 91−97.

2. Webster, T.J., Massa-Schlueter, E.A., Smith, J.L., and Slamovich, E.B., Osteoblast response to hydroxyapatite doped with divalent and trivalent cations, *Biomaterials,* 2004, vol. 25, pp. 2111−2121.

3. Narasaraju, T.S.B. and Phebe, D.E., Review: some physico-chemical aspects of hydroxylapatite, *J. Mater. Sci.,* 1996, vol. 3, pp. 11−21.

4. Zuev, V.P., Pankratov, A.S., and Alekseeva, A.N., Use of ultrafine hydroxyapatite particles in integrated treatment of mandibular fractures, *Stomatologiya,* 1994, no. 4, pp. 31−33.

5. Janning, C., Willbold, E., Vogt, C., Nellesen, J., Meyer-Lindenberg, A., Windhagen, H., Thorey, F., and Witte, F., Magnesium hydroxide temporarily enhancing osteoblast activity and decreasing the osteoclast number in peri-implant bone remodeling, *Acta Biomater.,* 2010, vol. 6, pp. 1861−1868.

6. Melikhov, I.V., Komarov, V.F., Severin, A.V., Bozhevol'nov, V.E., and Rudin, V.N., Two-dimensional crystalline hydroxyapatite, *Dokl. Phys. Chem.,* 2000, vol. 373, no. 3, pp. 125−128.

7. Suvorova, E.I. and Buffat, P.A., Electron diffraction from micro- and nanoparticles of hydroxyapatite, *J. Microsc.,* 1999, vol. 196, no. 1, pp. 46−58.

8. Shirley, D.A., High-resolution X-ray photoemission spectrum of the valence bands of gold, *Phys. Rev. B: Condens. Matter Mater. Phys.,* 1972, vol. 5, pp. 4709−4714.

9. Nefedov, V.N., *Rentgenoelektronnaya spektroskopiya khimicheskikh soedinenii* (X-ray Photoelectron Spectroscopy of Chemical Compounds), Moscow: Khimiya, 1984.

10. Sosulnikov, M.I. and Teterin, Yu.A., X-ray photoelectron studies of Ca, Sr, Ba and their oxides and carbonates, *J. Electron Spectrosc. Relat. Phenom.,* 1992, vol. 59, pp. 111−126.

11. *NIST X-ray Photoelectron Spectroscopy Database, Version 4.1,* Gaithersburg: National Inst. of Standards and Technology, 2012).
https://doi.org/10.18434/T4T88K

Translated by O. Tsarev

SPELL: 1. OK